Calibration of Star Formation Rate Tracers using Evolutionary Synthesis Models

H. Otí-Floranes and J.M. Mas-Hesse

Abstract Starburst phenomena can be characterized by their Star Formation Rate, which measures the mass converted to stars per unit time within the starburst region. Many diverse expressions for this magnitude, using the emission of the bursts at different wavelengths, have been suggested in the literature: UV radiation emitted by young stars, FIR emission from dust heated by the UV field, recombination lines from the gas nebula surrounding the stars, X-ray emission from X-ray binaries, etc... Our objective is to use last generation evolutionary synthesis models to calibrate the different Star Formation Rate (for constant stellar formation bursts), or Star Formation Strength (for instantaneous bursts) tracers in a consistent way. The first step performed has been to derive the calibration of the soft X-ray luminosity as a Star Formation Rate/Strength tracer. In this contribution we present the same kind of analyses performed on several other tracers at lower energies, such as the UV continuum, the production of ionizing photons per unit of time, the total infrared emission, etc. We also compare the expressions yielded by the models with those frequently used in the literature and discuss the ranges of usability of the latter ones. Several results are presented, among which we stress the importance of taking into account both the age of the burst considered, as well as the type of burst (extended or instantaneous) for the sources studied.

H. Otí-Floranes
Laboratorio de Astrofísica Espacial y Física Fundamental, CAB (CSIC–INTA), POB 78, 28691 Villanueva de la Cañada, Spain, and Dpto. de Física Moderna, Facultad de Ciencias, Universidad de Cantabria, 39005 Santander, Spain, e-mail: otih@laeff.inta.es

J.M. Mas-Hesse
Laboratorio de Astrofísica Espacial y Física Fundamental, CAB (CSIC–INTA), POB 78, 28691 Villanueva de la Cañada, Spain, e-mail: mm@laeff.inta.es

1 Introduction

The emission of radiation in most of the electromagnetic range in a star-forming galaxy is dominated by a starburst. The UV and optical domains are controlled by massive stars, and their ionizing radiation causes the nebular gas which surrounds the stars to emit conspicous recombination lines. Dust particles are heated when absorbing part of the UV field, producing the FIR (far infrared) radiation that dominates this energy range over any other source whatsoever. Radio emission is present as well, both in thermal and non-thermal nature, being the former a byproduct of free-free transitions within the nebular gas, whereas the latter appears when electrons are accelerated by SNRs (supernova remnants) and emit synchrotron radiation. Also, mechanical energy injected into the medium by SNe (supernovae) and stellar winds can heat the surrounding gas up to temperatures of millions of Kelvin, causing it to radiate in the X-rays range. Therefore, physical magnitudes which quantify all these different emissions can be used as *SFR* (star formation rate) estimators [4, 11, 3, 10]. Similarly to the study carried out in [7] for soft X-rays luminosity, here we present the calibration performed on lower energy tracers of star formation: $L_{\rm FIR}$, the continuum luminosity at 1500, 2000, 3500, 4400, 5500 and 22200 Å, the number of ionizing photons emitted per second ($N_{\rm Lyc}$), the luminosities $L(\mathrm{H}\alpha)$ and $L(\mathrm{Ly}\alpha)$, and the mechanical energy injected into the medium per second ($\dot{E}_K$).

Table 1 *SFS* estimators. Values by which magnitudes values should be multiplied in order to obtain *SFS*.

Magnitude	IB (4 Myr)	IB (5 Myr)	IB (6 Myr)
$L_{\rm FIR}$ (erg s^{-1}M$_\odot{}^{-1}$)	1.7×10^{-37}	2.5×10^{-37}	3.5×10^{-37}
$N_{\rm Lyc}$ (s^{-1} M$_\odot{}^{-1}$)	6.7×10^{-47}	1.0×10^{-46}	4.5×10^{-46}
$L(\mathrm{H}\alpha)$ (erg s^{-1}M$_\odot{}^{-1}$)	4.9×10^{-35}	7.4×10^{-35}	3.3×10^{-34}
$L(\mathrm{Ly}\alpha)_{\rm int}$ (erg s^{-1}M$_\odot{}^{-1}$)	4.1×10^{-36}	6.2×10^{-36}	2.8×10^{-35}
$L(\mathrm{Ly}\alpha)_{\rm corr}$ (erg s^{-1}M$_\odot{}^{-1}$)	4.1×10^{-35}	6.2×10^{-35}	2.8×10^{-34}
$\dot{E}_K$ (erg s^{-1}M$_\odot{}^{-1}$)	1.1×10^{-35}	1.4×10^{-35}	2.0×10^{-35}
$L_{\rm softX}$ (erg s^{-1}M$_\odot{}^{-1}$)	-	2×10^{-34}	-
L_{1500} (erg s^{-1}Å^{-1} M$_\odot{}^{-1}$)	3.3×10^{-34}	5.0×10^{-34}	6.9×10^{-34}
L_{2000} (erg s^{-1}Å^{-1} M$_\odot{}^{-1}$)	6.7×10^{-34}	1.1×10^{-33}	1.5×10^{-33}
L_{3500} (erg s^{-1}Å^{-1} M$_\odot{}^{-1}$)	2.8×10^{-33}	4.9×10^{-33}	7.0×10^{-33}
L_{4400} (erg s^{-1}Å^{-1} M$_\odot{}^{-1}$)	4.2×10^{-33}	6.1×10^{-33}	5.8×10^{-33}
L_{5500} (erg s^{-1}Å^{-1} M$_\odot{}^{-1}$)	8.3×10^{-33}	9.0×10^{-33}	8.6×10^{-33}
L_{22200} (erg s^{-1}Å^{-1} M$_\odot{}^{-1}$)	7.8×10^{-31}	3.4×10^{-31}	2.5×10^{-31}

2 Evolutionary synthesis models

The synthesis models used were CMHK02 [6, 2] and SB99 [5], for which we assumed solar metallicity ($Z = 0.020$) and a Salpeter IMF (Initial Mass Function)

with $2-120$ $M_\odot$ as mass limits for the nominal model. We considered the Geneva standard mass-loss tracks to compute the evolution of the magnitudes values for either an EB (Extended Burst, constant star formation) model or an IB (Instantaneous Burst) model. These models are characterized by *SFR* and by the initial mass of the burst (*SFS*, Star Formation Strength) respectively. Magnitudes are scaled to any one of them, depending on the model considered.

In order to calculate $L_{\rm FIR}$, we assumed thermal equilibrium in the dust grains, a Cardelli extinction law with $R_V = 3.1$ and *E(B-V)*$= 1$ [1], and absorption of 30% ionizing photons. As [7] showed, there is saturation when considering *E(B-V)*$>$ 0.5, thus we took *E(B-V)*$= 1$ as nominal. When calculating $N_{\rm Lyc}$, we applied the f-correction, which involves rejecting 30% of ionizing photons, which are absorbed by dust.

3 Results and discussion

In Tables 1 and 2 we show the inverse of the scaled values of the different magnitudes studied at different ages of the burst. These are the values by which the magnitudes values should be multiplied in order to obtain either *SFR* or *SFS*. The effect of the age is clearly visible, especially in IB models. The ages were selected so that the typical time band for both EB and IB models was covered. Besides $N_{\rm Lyc}$,

Table 2 *SFR* estimators. Values by which magnitudes values should be multiplied in order to obtain *SFR*.

Magnitude	EB (10 Myr)	EB (30 Myr)	EB (250 Myr)
$L_{\rm FIR}$ (erg s^{-1}(M$_\odot$ yr^{-1})$^{-1}$)	1.9×10^{-44}	1.5×10^{-44}	1.2×10^{-44}
$N_{\rm Lyc}$ (s^{-1}(M$_\odot$ yr^{-1})$^{-1}$)	4.1×10^{-54}	4.1×10^{-54}	4.1×10^{-54}
$L(\mathrm{H}\alpha)$ (erg s^{-1}(M$_\odot$ yr^{-1})$^{-1}$)	3.0×10^{-42}	3.0×10^{-42}	3.0×10^{-42}
$L(\mathrm{Ly}\alpha)_{\rm int}$ (erg s^{-1}(M$_\odot$ yr^{-1})$^{-1}$)	2.5×10^{-43}	2.5×10^{-43}	2.5×10^{-43}
$L(\mathrm{Ly}\alpha)_{\rm corr}$ (erg s^{-1}(M$_\odot$ yr^{-1})$^{-1}$)	2.5×10^{-42}	2.5×10^{-42}	2.5×10^{-42}
$\dot{E}_K$ (erg s^{-1}(M$_\odot$ yr^{-1})$^{-1}$)	2.2×10^{-42}	1.1×10^{-42}	9.9×10^{-43}
$L_{\rm softX}$ (erg s^{-1}(M$_\odot$ yr^{-1})$^{-1}$)	8×10^{-41}	2×10^{-41}	-
L_{1500} (erg s^{-1}Å^{-1}(M$_\odot$ yr^{-1})$^{-1}$)	4.1×10^{-41}	3.3×10^{-41}	2.7×10^{-41}
L_{2000} (erg s^{-1}Å^{-1}(M$_\odot$ yr^{-1})$^{-1}$)	8.4×10^{-41}	6.6×10^{-41}	5.1×10^{-41}
L_{3500} (erg s^{-1}Å^{-1}(M$_\odot$ yr^{-1})$^{-1}$)	3.4×10^{-40}	2.6×10^{-40}	1.8×10^{-40}
L_{4400} (erg s^{-1}Å^{-1}(M$_\odot$ yr^{-1})$^{-1}$)	6.5×10^{-40}	4.2×10^{-40}	2.2×10^{-40}
L_{5500} (erg s^{-1}Å^{-1}(M$_\odot$ yr^{-1})$^{-1}$)	1.1×10^{-39}	7.2×10^{-40}	3.6×10^{-40}
L_{22200} (erg s^{-1}Å^{-1}(M$_\odot$ yr^{-1})$^{-1}$)	2.3×10^{-38}	1.2×10^{-38}	6.7×10^{-39}

we display the calibration for $L(\mathrm{H}\alpha)$ and $L(\mathrm{Ly}\alpha)$, assuming for the former $T_{\rm e} = 10^4$ K and $N_{\rm e} = 10^2$ cm^{-3} [8] and for the latter one Lyα photon emitted per ionization event. For $L(\mathrm{Ly}\alpha)$ we show two values: the intrinsic one $L(\mathrm{Ly}\alpha)_{\rm int}$ and the value $L(\mathrm{Ly}\alpha)_{\rm corr}$ that would be observed considering that just 10% of the emission escaped from the burst, which is the fraction typically observed [9].

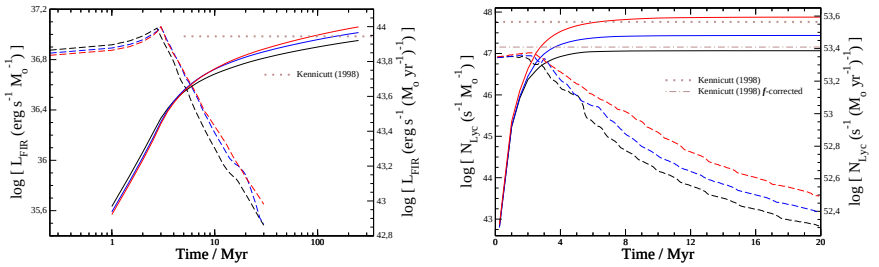

Fig. 1 Evolution of $L_{\rm FIR}$ (left) and $N_{\rm Lyc}$ (right) predicted by CMHK02 for IB models (dashed line, left axis, normalized to $SFS = 1\ {\rm M}_\odot{}^{-1}$) and by SB99 ($L_{\rm FIR}$) and CMHK02 ($N_{\rm Lyc}$) for EB models (solid line, right axis, normalized to $SFR = 1\ {\rm M}_\odot\ {\rm yr}^{-1}$) as a function of metallicity (from bottom to top: $Z = 0.020$, 0.008, 0.001), together with the values taken from [4].

The expressions for *SFR* taken from [4] and [11] were compared to the predictions of the models. These calibrations from the literature assume mass limits for the IMF different from ours ($0.1 - 100\ {\rm M}_\odot$), and hence a correction is needed to make the comparison possible. This correction is two fold [12]: 1) the scaled values from the models are $M_{0.1}^{100}/M_2^{120} = 3.4135$ larger than the ones yielded by the published calibrations, and 2) the number of massive stars relative to the total number is higher in our models. This can be amended studying the ratio of the observables for two models, one with each IMF limits, after the first effect has been corrected.

The general evolution of the magnitudes for IB models follows a rather constant value or a small raise during the first ~ 3 Myr, after which massive stars start to die and the magnitudes decrease. On the contrary, for EB models we observe a steep increase during the first Myrs, which later flattens, until a somewhat steady state is reached, when an equilibrium exists between death and creation of stars. In Figs. 1, 2 and 3 we can observe these behaviours, as well as the impact of age and metallicity on the magnitudes shown.

In the evolution of $L_{\rm FIR}$, L_{1500} and $\dot{E}_K$ we observe a decrease of ~ 0.7, ~ 0.7 and ~ 0.5 dex respectively within 4 Myr after the death of the first stars for IB models, whereas the fall in $N_{\rm Lyc}$ is even higher, being one order of magnitude in only ~ 2.5 Myr. The behaviour of L_{4400} and L_{5500} is different due to the importance of the emission of WR stars in these magnitudes, which casues, as we show in Fig. 3, a hump not observed in the previous observables, after a prior increase of 0.3 dex in the values of the luminosities. This hump is quite bumpy, showing a scatter of 0.3 and 0.25 dex for L_{4400} and L_{5500}, respectively.

On the other hand, for EB models we observe a steep initial raise of 0.7 dex during $4 - 5$ Myr and a weaker increase of 0.3 dex afterwards up to 250 Myr in the evolution of $L_{\rm FIR}$, L_{1500} and L_{3500}. The values in the raises for L_{4400} and L_{5500} are higher, being 1 dex for the first regime and 0.6 and 0.7 dex for the second one, respectively. A rapid approach to the steady state is observed in the evolution of $N_{\rm Lyc}$, which, after an increase of one order of magnitude during the first 8 Myr after the onset of the burst, remains constant. In the case of $\dot{E}_K$, it takes ~ 40 Myr to reach

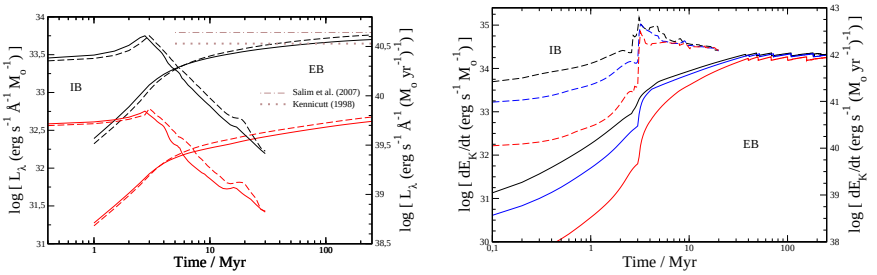

Fig. 2 Evolution of L_{1500} and L_{3500} (left) and $\dot{E}_K$ (right) predicted by CMHK02 for IB models (left axis, normalized to $SFS = 1$ M$_\odot{}^{-1}$) and by SB99 for EB models (right axis, normalized to $SFR = 1$ M$_\odot$ yr^{-1}) as a function of metallicity. Left: $Z = 0.020$ (solid) and 0.008 (dashed), L_{1500} on top, together with the values taken from [4] and [11]. Right: from top to bottom: $Z = 0.020$, 0.008, 0.001.

the steady state, subsequent to a steep raise of ~ 1.7 dex during the first 3 Myr and of ~ 1.3 dex during the next ~ 35 Myr.

The dependance of the different magnitudes with respect to metallicity is rather varied, both due to the model assumed and to the magnitudes considered. If we compare the models with solar metallicity to those with $Z = 0.008$, we find that for IB models, there is medium dependance ($\sim 25\%$) for L_{1500}, $L_{\rm FIR}$ and L_{4400}. It is somewhat higher for L_{3500} and L_{5500} ($\sim 60\%$) and much higher for $\dot{E}_K(0.2-0.4$ dex). The influence of Z is weaker in EB models, being around 10% and even lower, except for $N_{\rm Lyc}$, which is $\sim 25\%$.

When assuming a lower value for Z, lifetimes of stars become longer, which explains the larger values for the continuum luminosities, $L_{\rm FIR}$ and $N_{\rm Lyc}$. For $\dot{E}_K$ it works the other way, since the power of stellar winds increase with Z. However, when SNe dominate over winds, like in EB models for ages > 40 Myr, this trend disappears.

Contrary to what [4] states, his SFR(FIR) calibration does not apply for bursts with ages lower that 100 Myr, but larger than this age, attending to our models, as can be seen in Fig. 1. In fact, using his expression in the range $100-250$ Myr entails an error ≤ 15 %. His calibration of $SFR(N_{\rm Lyc})$ agrees well for ages > 8 Myr once it has been f-corrected, otherwise SFR is underestimated by $\sim 30\%$. Also, we show in Fig. 2 the value predicted for L_{1500} by his SFR(UV) calibration and, although [4] affirms that it should be used for bursts older than 100 Myr, there is little error ($< 12\%$) in applying it to bursts older than 30 Myr. Also, we compared our predictions with the value given by the calibration performed by [11], which underestimates SFR compared to our models due to several facts: 1) their models assumed a different SFH (star formation history), 2) the average metallicity of the sample used is $Z = 0.016$ and 3) the sample has an intrinsic scatter in the SFH.

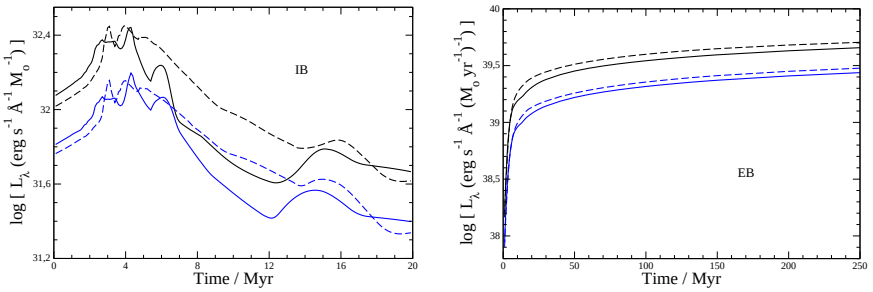

Fig. 3 Evolution (from top to bottom) of L_{4400} and L_{5500} predicted by CMHK02 for IB models (left, normalized to $SFS = 1$ $M_{\odot}{}^{-1}$) and by SB99 for EB models (right, normalized to $SFR = 1$ $M_{\odot}$ yr^{-1}) both for $Z = 0.020$ (solid line) and $Z = 0.008$ (dashed line).

4 Conclusions

We have obtained robust calibrations of *SFR* and *SFS* based on several tracers using last generation synthesis models. As we have shown, a total different behaviour is expected between instantaneous bursts and processes with constant star formation, and hence care should be taken when choosing the right model to reproduce the properties of the sources studied. Also, we have stressed the importance of the age effect, provoking that *SFR* and *SFS* expressions should be given for a band of ages, instead of being used regardless the evolutionary state of the burst, as is usually done in the literature. A quantitative description of the effect of metallicty in the tracers has been given, together with the explanation of such dependencies. Finally, we have provided [4] *SFR* calibrations with an age range within which they can be used with little error attending to our models.

HO and JMMH are funded by Spanish MEC grants ESP2005-07714-C03-03.

References

1. Cardelli, J. A., Clayton, G. C., & Mathis, J. S. 1989, ApJ, 345, 245
2. Cerviño, M., & Mas-Hesse, J. M. 1994, ApJ, 284, 749
3. Condon J. J., 1992, ARA&A, 30, 575
4. Kennicutt R. C., Jr., 1998, ARA&A, 36, 189
5. Leitherer, C., et al. 1999, ApJS, 123, 3
6. Mas-Hesse, J. M., & Kunth, D. 1991, A&AS, 88, 399
7. Mas-Hesse, J. M., Otí-Floranes, H., & Cerviño, M. 2008, A&A, 483, 71
8. Osterbrock, D. E. 1989, "Astrophysics of Gaseous Nebulae and Active Galactic Nuclei", University Science Books, California
9. Östlin, G., Hayes, M., Kunth, D., Mas-Hesse, J. M., Leitherer, C., Petrosian, A., & Atek, H. 2008, ArXiv e-prints, 803
10. Ranalli, P., Comastri, A., & Setti, G. 2003, A&A, 399, 39
11. Salim, S., et al. 2007, ApJS, 173, 267
12. Wilkins, S. W., Hopkins, A. M., Trentham, N., & Tojeiro, R. 2008, ArXiv e-prints, 809